NJC

Accepted Manuscript

This is an *Accepted Manuscript*, which has been through the Royal Society of Chemistry peer review process and has been accepted for publication.

Accepted Manuscripts are published online shortly after acceptance, before technical editing, formatting and proof reading. Using this free service, authors can make their results available to the community, in citable form, before we publish the edited article. We will replace this *Accepted Manuscript* with the edited and formatted *Advance Article* as soon as it is available.

You can find more information about *Accepted Manuscripts* in the Information for Authors.

Please note that technical editing may introduce minor changes to the text and/or graphics, which may alter content. The journal's standard Terms & Conditions and the Ethical guidelines still apply. In no event shall the Royal Society of Chemistry be held responsible for any errors or omissions in this *Accepted Manuscript* or any consequences arising from the use of any information it contains.

ROYAL SOCIETY OF CHEMISTRY

www.rsc.org/njc

Cite this: DOI: 10.1039/c0xx00000x

www.rsc.org/xxxxxx

ARTICLE TYPE

New Benzoxazines Containing Polyhedral Oligomeric Silsesquioxane from Eugenol, Guaiacol and Vanillin

Thirukumaran Periyasamy, ShakilaParveen Asrafali and Sarojadevi Muthusamy*

Received (in XXX, XXX) Xth XXXXXXXXX 20XX, Accepted Xth XXXXXXXXX 20XX
DOI: 10.1039/b000000x

Abstract

Polybenzoxazine-tethered polyhedral oligomeric silsesquioxane nanocomposites with well-defined architecture were prepared by the reaction of bio-phenols: eugenol, guaiacol, vanillin; poss-octaamine with paraformaldehyde. FT-IR measurements evidenced the occurrence of Mannich reaction between phenolic group of bio-phenols and amino group of POSS molecule, with the consequent formation of a heterocyclic benzoxazine ring binding POSS in its backbone. Their chemical structures were proved by ^{1}H and ^{13}C-NMR analysis. Thermo-mechanical properties and thermal stability of the POSS-polybenzoxazine hybrid networks were determined by DSC, DMA and TGA. SEM, EDX, AFM and TEM micrographs show that POSS-Pbz nanocomposites exhibit featureless morphologies with no discernible phase separation, suggesting that the POSS nanoparticles are dispersed homogeneously throughout the matrix. The homogeneity of these networks with octafunctional POSS is also indicated by their moduli in the range of 2.63 to 2.91 GPa. Moreover, their dielectric values [both dielectric constant (1.85) and dielectric loss (0.28)] and moisture absorption values are very low (<0.01%) which makes them suitable materials for use in microelectronics packaging.

Keywords: Bio-phenols, POSS-octaamine, hybrid network, microelectronics packaging.

1. Introduction

Organic-inorganic hybrid materials receive significant attention from polymer scientists, inspired by remarkable potential to combine two dramatically different material classes at the molecular level[1]. Since their introduction, composites have become important materials in terms of possessing new properties and exploiting unique synergism between the constituents[2]. Various methods were developed to prepare organic/inorganic polymer hybrids, including sol-gel techniques, co-polymerization with hybrid building blocks and post treatment of organic polymers. Significant enhancement in thermal, mechanical and physical properties of polymers can be achieved by incorporating a variety of nanofillers, such as carbon nanotubes, layered silicates and polyhedral oligomeric silsesquioxanes (POSS) into the polymer backbone. This class of materials is currently facing applications in a number of areas, including optics, electronics, mechanics, energy, environment, biology, medicine, catalysis, sensors etc[3,4].

Benzoxazines (Bzo) are a versatile class of thermoset resins synthesized by Mannich condensation between an aromatic alcohol, a primary amine and formaldehyde[5,6]. These resins are used as thermoset matrix for higher performance nanocomposites because of their higher mechanical and thermal properties[7]. The chemistry of benzoxazine synthesis offers wide molecular design flexibility and thus facilitates preparation of various polybenzoxazine-based composites. Many strategies have been developed with the aim of expanding the scope and circumventing the limitations of benzoxazine resins. These include (i) synthesis of benzoxazine monomers with additional functionality, (ii) incorporation of benzoxazine in polymer chains and (iii) synthesis of benzoxazine-based composites or alloys[2]. Benzoxazine-based composites can be of two types; (i) fiber-reinforced polybenzoxazine composites or (ii) inorganic particles reinforced polybenzoxazine (e.g. silica, TiO_2, magnetic nanoparticles).

In recent years, polyhedral oligomeric silsesquioxane (POSS) is emerging as a new type of additive that offers the possibility of nanoscale reinforcement and stabilization of polymers. POSS are typical molecular nanobuilding blocks, used to reinforce the polymer organic matrix for various applications, owing to the ease with which functional groups can be attached[8,9]. POSS molecules have a cage-shaped three dimensional structure. Among them, octasilsesquioxanes ($R_8Si_8O_{12}$) (n=8) have been mostly investigated as it consists of a rigid, cubic silica core, where each of the eight corners carries one organic group[6]. Unlike conventional inorganic fillers, POSS nanofillers offer the advantage of monodisperse size, low density and synthetically well-controlled functionalities. POSS itself is a hybrid material, being a well-defined spherosilicate polyhedral molecule possessing an inner cage diameter of approximately 0.5 nm. The tendency to aggregate is determined by the compatibility of POSS with the polymer matrix which is controlled by the organic substituents in the POSS framework[1,10]. Therefore, selecting an appropriate chemical group to modify POSS is the key to prevent aggregation of POSS and to obtain high-performance composites.

Incorporation of POSS macromer within the polymeric network allows the organic and inorganic phases to interact at the molecular level with assured compatibility[5].

Nowadays, the replacement of petroleum-based raw materials by using renewable resources has become a major challenge as these materials could lead to development of sustainable polymers from environmentally and energy favorable resources[11]. Renewables have the potential to provide sustainable supply of basic chemical building blocks. As natural resources become scarce, increasing concerns about the environment and sustainability are fueling a growing worldwide research effort devoted for understanding and using renewable materials/feedstocks[12].

This paper intends to explain the reinforcing effect of POSS on the bio based polybenzoxazines and the relationship between structure and properties of the POSS reinforced bio-based benzoxazines. Eugenol is a member of phenylpropanoids class of chemical compounds. It is clear to pale yellow oily liquid extracted from certain essential oils especially from clove oil, nutmeg, cinnamon, basil and bay leaf. Guaiacol is usually obtained by the pyrolysis of biomass like lignin. Its aromatic structure is acknowledged as a fundamental unit in lignin molecules. Vanillin is a naturally occurring phenol, extracted from the seed pods of vanilla planifola. It is identified as a sustainable and valuable chemical feedstock, containing a methoxy group at the ortho position and a formyl group at the para position of the phenol. In this article we have selected renewable raw materials such as eugenol, guaiacol and vanillin as bio-phenols which were reacted with octaamine functionalized POSS and paraformaldehyde to synthesize fully renewable POSS-polybenzoxazine nanocomposites with superior properties. The degree of dispersion and the size of POSS in the POSS-Pbz nanocomposites were characterized. The thermo-mechanical properties, thermal stability and dielectric properties of these hybrid systems were also examined.

2. Experimental

2.1. Materials

Eugenol was purchased from Alfa Aesar (Johnson Mathew Company) Pvt. Ltd.; guaiacol was purchased from Spectrochem Pvt. Ltd.; vanillin was purchased from Sigma-aldrich Pvt. Ltd.; paraformaldehyde and ethanol were purchased from Merck Specialities Pvt. Ltd., India; dimethylsulphoxide (DMSO), methanolic solution (40%) of benzyltrimethylammonium hydroxide, triethylamine, benzene, tetrahydrofuran (THF) and 10% Pd/C were purchased from Sisco Research Laboratories Pvt. Ltd. India; phenyltrichlorosilane was purchased from Aldrich, India.

2.2. Characterization methods

Fourier transform infrared (FTIR) spectra of the samples were obtained using an ABB Bomem (Model MB3000) spectrometer. The cured samples were ground with spectroscopic grade KBr and made into pellets. ^{1}H (500 MHz), nuclear magnetic resonance (NMR) spectra were recorded on a JEOL spectrometer with tetramethylsilane (TMS) as the internal standard. Solutions were prepared in DMSO-d_6. Differential scanning calorimetry was performed in a TA instrument Q_{10} model using 5-10 mg of the sample at a heating rate of 10^{o}C/min in nitrogen atmosphere. Dielectric constant and dielectric loss measurements were carried out with an impedance analyzer (Solatron 1260 Impedance/Gain-phase Analyzer) at room temperature. The polymer samples were made in the form of pellets (1 mm thickness × 12 mm dia.) using platinum (Pt) electrode sandwich model in the frequency range of 10 Hz - 1 MHz at room temperature. The dielectric constant and dielectric loss of the samples were determined using ε′ and ε" as standard relations. The morphology of the material was examined by scanning electron microscope (SEM) (JEOL, JSM-5600) at an accelerating voltage of 20 kV. The surface topology (roughness) of the fractured surface was investigated by means of atomic force microscopy (AFM) Seiko SPI3800N, series SPA-400 (Tokyo, Japan). High resolution transmission electron microscopic (HR-TEM) images were recorded using JOEL, JEM 2100 electron microscope operated at 200 kV. Dynamic mechanical analysis (DMA) was carried out using a Netzsch 242 DMA at a heating rate of 10 ^{o}C/min from 30 to 250 ^{o}C. For moisture absorption measurements, specimens with dimensions 63 x 13 x 3 mm^3 were cut from the POSS-Pbz nanocomposites and placed in water bath and in open air at room temperature for 1 week. At regular intervals (Day 1 and Day 7), each sample was first removed from water and dried with a tissue paper before weighing. The percentage of weight change (from both water and air) for the specimen was determined.

2.3. Synthesis Procedures

2.3.1. Synthesis of octa(aminophenyl) silsesquioxane (OAPS)

Octa(aminophenyl) silsesquioxane was synthesized from octaphenyl silsesquioxane (OPS) by following the reported method[13].

2.3.1.1. Octaphenyl silsesquioxane (OPS)

FT-IR (KBr, cm^{-1}): 3160 - 2850 (C-H stretching), 1250 - 980 (Si-O-Si stretching), 735 & 507 (C-H bending).

2.3.1.2. Octa (nitrophenyl) silsesquioxane (ONPS)

FT-IR (KBr, cm^{-1}): 3160-2850 (C-H stretching), 1527 & 1340 (N-O stretching), 1250-975 (Si-O-Si stretching), 735 & 507 (C-H bending).

2.3.1.3. Octa(aminophenyl) silsesquioxane (OAPS)

FT-IR (KBr, cm^{-1}): 3355 (N-H stretching), 3125-2825 (C-H stretching), 1600 (C-C stretching), 1438 (C-H stretching), 1220-964 (Si-O-Si stretching), 690 & 495 (C-H stretching); ^{1}H-NMR (acetone-d_6, ppm): 7.3-6.2 (m, aromatic), 4.4 (s, amine); ^{13}C-NMR (acetone-d_6, ppm): 153.2, 151.6, 138.3, 134.1, 131.9, 123.2, 120.8, 118.8, 116.2, 115.4 (aromatic carbons). FT-IR, ^{1}H NMR, ^{13}C NMR and ^{29}Si NMR of OAPS are given in supporting information.

2.3.2. Synthesis of benzoxazine monomers

2.3.2.1. Synthesis of POSS-Eugenol based benzoxazine [POSS-EBzo]

In a 500 mL three necked round bottomed flask OAPS (0.001 m, 1.15 g) eugenol (0.008 m, 1.31 g) and 50 mL of DMSO were taken and stirred well to get a homogenous solution. Paraformaldehyde (0.016 m, 0.5 g) was added to the solution and the mixture was heated at 130 ^{o}C for 5h in an oil bath, cooled and finally poured into 250 ml of 1N aqueous sodium hydroxide solution. The precipitate formed was collected by filtration, washed several times with water. After drying at 60 ^{o}C in a vacuum oven, pale yellow powder (82% yield) was obtained. (Scheme 1)

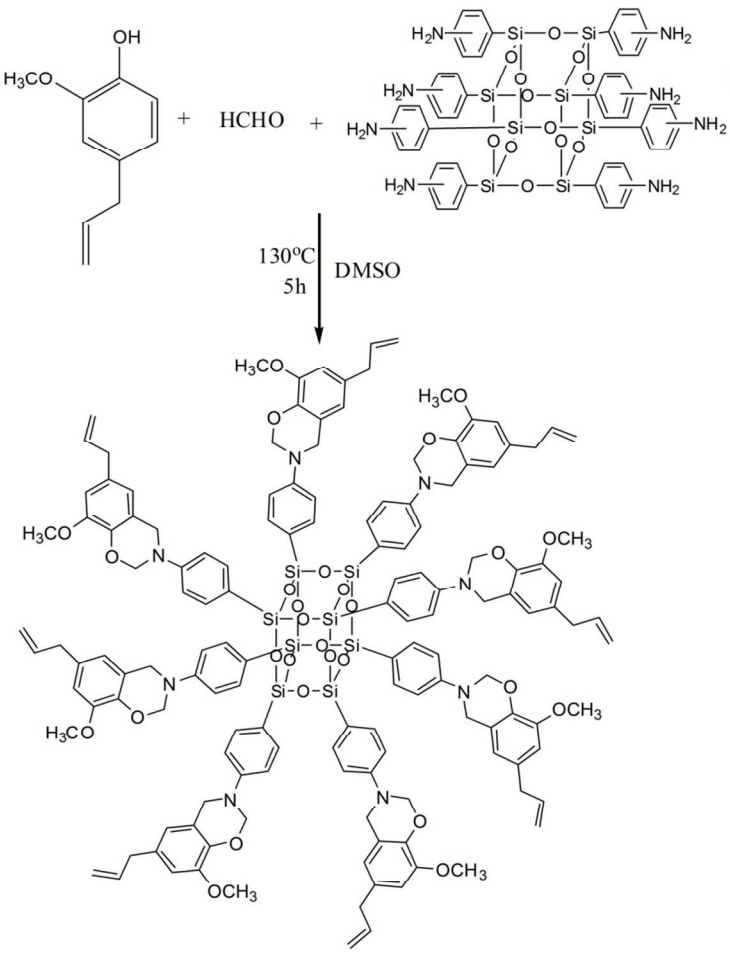

Scheme 1 Synthesis of POSS-Benzoxazine monomer (POSS-EBzo)

FT-IR (KBr, cm^{-1}): 2986 (C-H stretching), 1597 (C=C stretching), 1324 (CH_2 stretching), 948 (stretching vibrations of oxazine ring), 1109, 1227 and 1365 (C-O-C stretching), 1186 (C-N-C stretching); ^{1}H-NMR (DMSO-d_6, ppm): 4.6 (s, H_b, 16H), 5.4 (s, H_a, 16H), 3.7 (s, H_c, 24H), 3.2 (d, H_d, 16H), 5.9 (m, H_e, 8H), 5.1 (d, H_f, 16H), 6.5-8.0 (m, aromatic protons); ^{13}C-NMR (DMSO-d_6, ppm): 49.5 (Ar-CH_2-O), 79.9 (O-CH_2-N), 55.8 (-OCH_3), 115.6 (-$^{*}CH_2$-CH=CH_2), 138.2 (-CH_2-*CH=CH_2), 40.5 (-CH_2-CH=$^{*}CH_2$), 115-160 (aromatic carbons).

2.3.2.2. Synthesis of POSS-Guaiacol based benzoxazine [POSS-GBzo]

In a 500 mL three necked round bottomed flask OAPS (0.001 m, 1.15 g), guaiacol (0.008 m, 0.99 g) and 50 mL of DMSO were taken and stirred well to get a homogenous solution. Paraformaldehyde (0.016 m, 0.5 g) was added to the solution and the mixture was heated at 130 ^{o}C for 5h in an oil bath, cooled and finally poured into 250 ml of 1N aqueous sodium hydroxide solution. The precipitate formed was collected by filtration, washed several times with water. After drying at 60 ^{o}C in a vacuum oven, pale yellow powder (81% yield) was obtained. (Scheme 2)

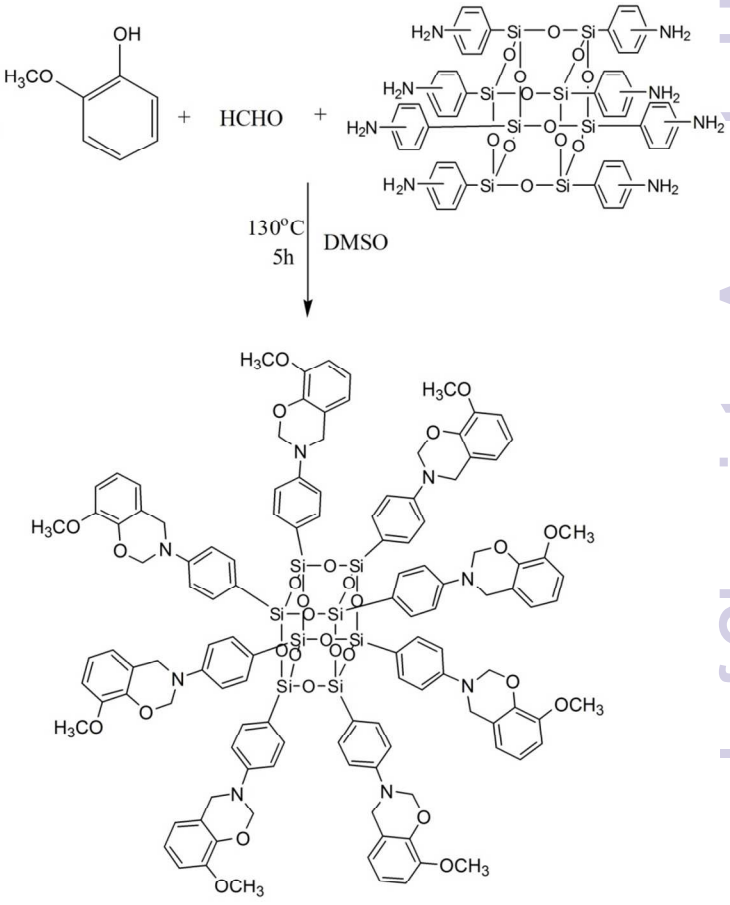

Scheme 2 Synthesis of POSS-Benzoxazine monomer (POSS-GBzo)

FT-IR (KBr, cm^{-1}): 2986 (C-H stretching), 1597 (C=C stretching), 1324 (CH_2 stretching), 945 (stretching vibrations of oxazine ring), 1108, 1225 and 1365 (C-O-C stretching), 1183 (C-N-C stretching); ^{1}H-NMR (DMSO-d_6, ppm): 4.5 (s, H_b, 16H), 5.4 (s, H_a, 16H), 3.7 (s, H_c, 24H), 6.5-8.0 (m, aromatic protons); ^{13}C-NMR (DMSO-d_6, ppm): 49.5 (Ar-CH_2-O), 79.9 (O-CH_2-N), 55.8(-OCH_3), 115-160 (aromatic carbons).

2.3.2.3. Synthesis of POSS-Vanillin based benzoxazine [POSS-VBzo]

In a 500 mL three necked round bottomed flask OAPS (0.001 m, 1.15 g) vanillin (0.008 m, 1.21 g) and 50 mL of DMSO were taken and stirred well to get a homogenous solution. Paraformaldehyde (0.016 m, 0.5 g) was added to the solution and the mixture was heated at 130 ^{o}C for 5h in an oil bath, cooled and finally poured into 250 ml of 1N aqueous sodium hydroxide solution. The precipitate formed was collected by filtration, washed several times with water and dried at 60 ^{o}C in a vacuum oven, pale yellow powder (83% yield) was obtained. (Scheme 3)

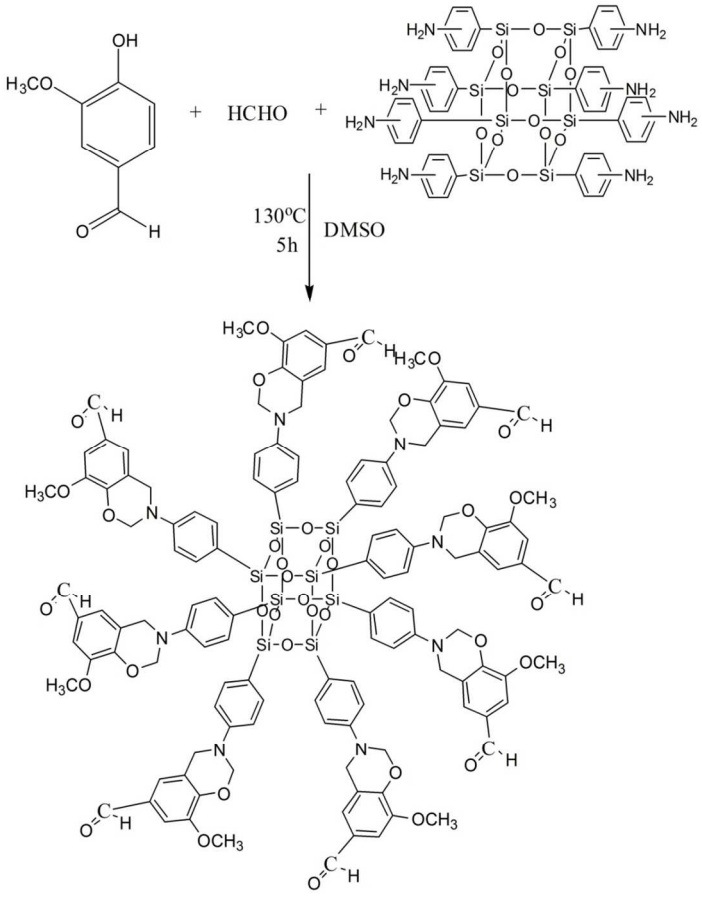

Scheme 3 Synthesis of POSS-Benzoxazine monomer (POSS-VBzo)

FT-IR (KBr, cm^{-1}): 2986 (C-H stretching), 1597 (C=C stretching), 1324 (CH_2 stretching), 938 (stretching vibrations of oxazine ring), 1112, 1222 and 1368 (C-O-C stretching), 1183 (C-C stretching); ^{1}H-NMR (DMSO-d_6, ppm): 4.6 (s, H_b, 16H), 5.5 (s, H_a, 16H), 3.7 (s, H_c, 24H), 9.7 (s, H_d, 8H) 6.5-8 (m, aromatic protons); ^{13}C-NMR (DMSO-d_6, ppm): 49.5 (Ar-CH_2-O), 79.9 (O-CH_2-N), 55.8(-OCH_3), 191.7 (-CHO),115-160 (aromatic carbons).

2.3.3. Preparation of POSS-Bzo nanocomposite for DMA analysis

Synthesized benzoxazine monomer (POSS-EBzo: 4.95 g) was dissolved in THF (10 ml) in a 100 mL beaker and stirred for 30 min at room temperature and stirred for 5h in open air to evaporate most of the THF. The solution was poured into the mould and cured at 100 ^{o}C/1h, 150 ^{o}C/1h, 200 ^{o}C/1h and then post cured at 250 ^{o}C for 1h. The cured samples were red wine colored with 3 mm thickness. Similar procedure was adopted for the preparation of other composites.

3. Results and Discussion

3.1. Structural Analysis

Chemical structure of the monomers was confirmed by FT-IR, ^{1}H NMR and ^{13}C NMR spectral methods.

Eugenol based benzoxazine monomer (POSS-EBzo) was synthesized by the condensation reaction of eugenol with formaldehyde and amine as shown in Scheme 1. The FT-IR spectrum (Fig.1) of this monomer shows characteristic absorption bands at 1233 cm^{-1} (asymmetric stretching of C-O-C), 1029 cm^{-1} (symmetric stretching of C-O-C) and 942 cm^{-1} (stretching vibrations of oxazine ring)[14]. The spectrum also shows a band at 1376 cm^{-1} due to tetra substituted benzene ring. Other aromatic vibrations are observed at 1593 and 1504 cm^{-1}. C-H stretching vibration of benzene ring appears at 3068 cm^{-1} and the peaks at 2934 and 2899 cm^{-1} are owing to the asymmetric and symmetric stretching vibrations of the methylene group of the oxazine ring as well as alkyl side chain of eugenol[15,16]. For POSS-GBzo and POSS-VBzo monomer the oxazine ring vibrations appear at 945 and 938 cm^{-1} respectively. The band for trisubstituted benzene ring in POSS-GBzo appears at 1464 cm^{-1}, whereas POSS-VBzo is tetrasubstituted whose band appears at 1371 cm^{-1}.

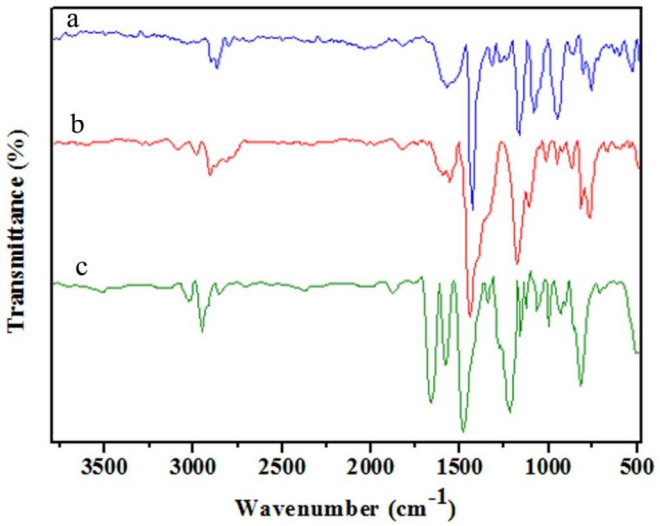

Figure 1 FTIR spectra of the POSS-Bzo monomers a) POSS-EBzo b) POSS-GBzo and c) POSS-VBzo

Figure 2 shows the ^{1}H-NMR spectra of all the benzoxazine monomers. The characteristic oxazine ring protons for POSS-EBzo appear as two singlets at 4.6 and 5.4 ppm which are assigned to Ar-CH_2-N and O-CH_2-N respectively[15]. The singlet at 3.7 ppm is due to the –OCH_3 protons. The doublets at 3.2 & 5.1 ppm (H_d and H_f protons) and the multiplet at 5.9 ppm (H_e protons) are assigned to allyl protons [-CH_2=CH-CH_2-]. The multiplets between 6.5 and 8.0 ppm are assigned to the aromatic protons. For POSS-GBzo and POSS-VBzo, the oxazine ring protons appear as two singlets at 4.5 & 5.4 ppm and at 4.6 & 5.5 ppm respectively. In case of POSS-VBzo, there is an additional peak for –CHO proton which appears at 9.7 ppm respectively.

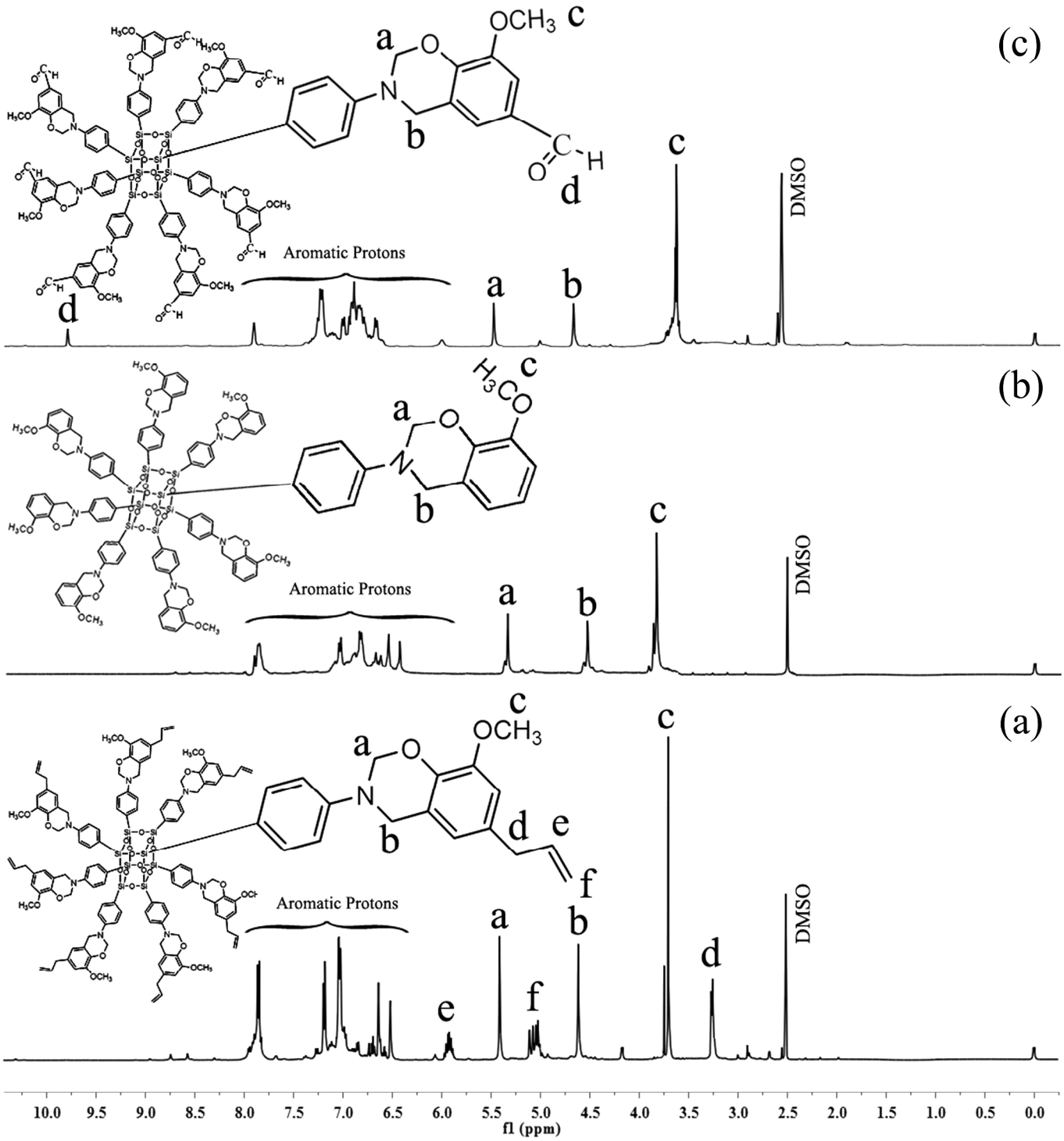

Figure 2 ^{1}H NMR spectra of the POSS-Bzo monomers a) POSS-EBzo b) POSS-GBzo and c) POSS-VBzo

Figure 3 shows the ^{13}C-NMR spectra of all the monomers. The characteristic carbon resonances of the oxazine ring for POSS-EBzo are found at 49.5 and 79.1 ppm for Ar-CH_2-N and O-CH_2-N respectively[17]. The peak at 55.9 ppm is attributed to the -OCH_3 carbon and the peaks at 115.8 ('d' carbons), 138.2 ('e' carbons) and 40.4 ppm ('f' carbons) are assigned to allyl carbons [CH_2=CH-CH_2-]. Whereas for POSS-GBzo and POSS-VBzo, the oxazine ring carbons appear as two singlets at 49.5 & 79.9 ppm respectively. For POSS-VBzo, there is an additional peak for –CHO carbon which appears at 191.7 ppm respectively.

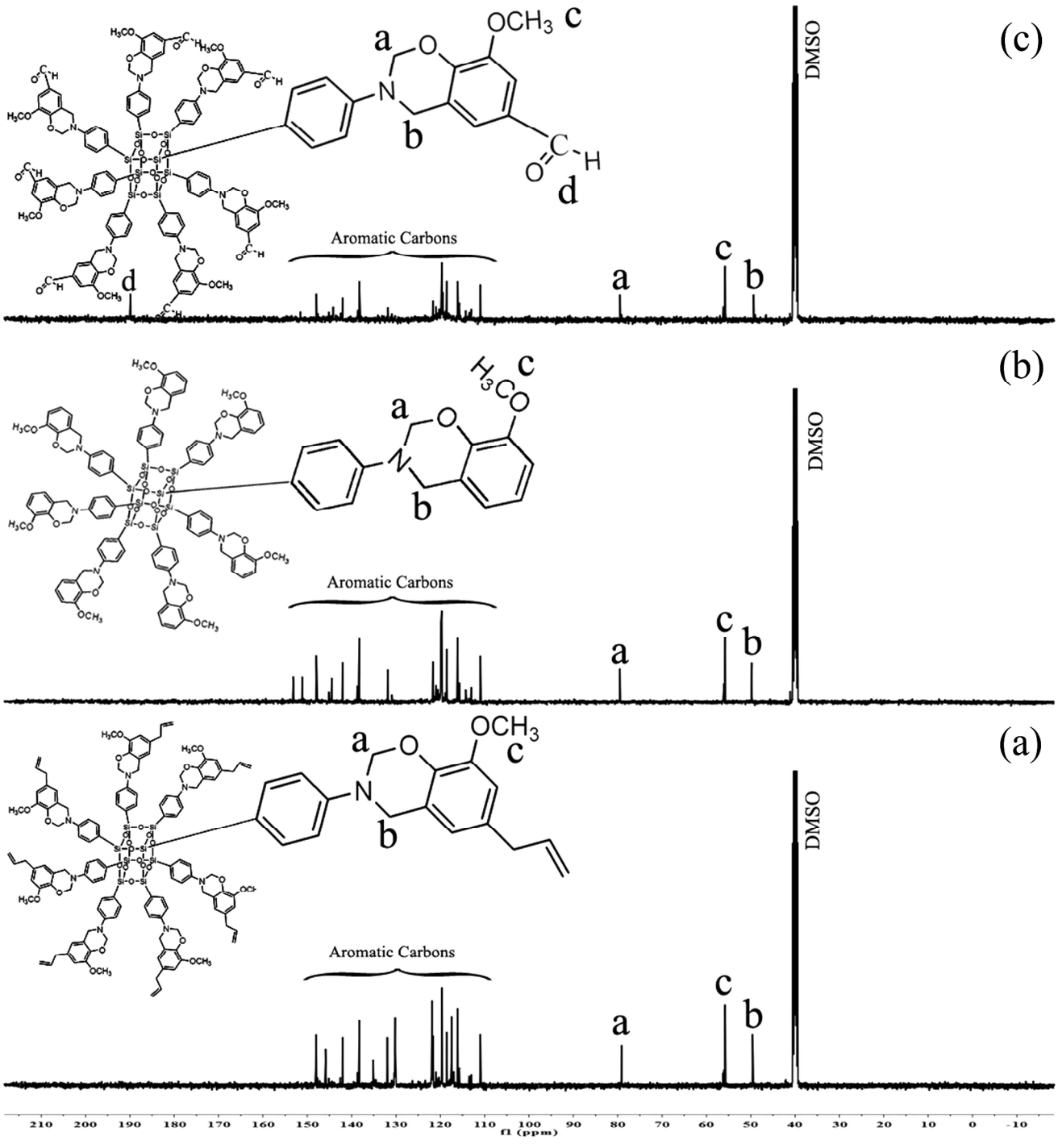

Figure 3 ^{13}C NMR spectra of the POSS-Bzo monomers a) POSS-EBzo b) POSS-GBzo and c) POSS-VBzo

3.2. Polymerization behavior of POSS-BZO monomers

The polymerization behavior of POSS-Bzo monomer was studied by DSC and FT-IR analysis.

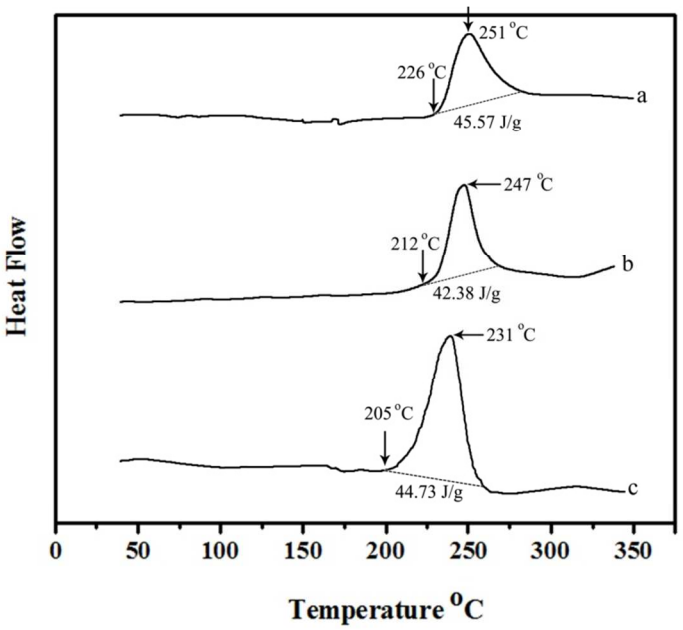

Figure 4 DSC thermograms of POSS-Bzo monomers a) POSS-EBzo b) POSS-GBzo and c) POSS-VBzo

Figure 4 shows the DSC plots for POSS-EBzo, POSS-GBzo and POSS-VBzo monomers recorded at a heating rate of 10 °C/min. The DSC thermograms show an exothermic peak with an onset at 226, 212 and 205 °C and cure maximum at 251, 247 & 231 °C for POSS-EBzo, POSS-GBzo and POSS-VBzo respectively. On comparison POSS-VBzo monomer shows lower curing temperature than the other two. This could be attributed to the presence of –CHO group in its backbone structure[10]. Reports have shown that this formyl group tends to oxidize easily forming carboxylic group which catalyze the ring-opening polymerization of benzoxazines. Moreover, their curing temperatures are similar to that of commercial benzoxazines which generally exhibits exothermic ring-opening reaction between 200-250 °C[18,19]. The possible structure of the cured polymer [POSS-EPbz] is shown in Scheme 4.

The curing reaction of the monomers was further confirmed by FT-IR analysis. Figure 5 shows the FT-IR spectra of the monomers after heating at 100, 150, 200 & 250 °C for 1h at each temperature. The characteristic absorption bands at 948 cm^{-1} (out of plane bending vibration of C-H) and 1465 cm^{-1} (trisubstituted benzene ring) gradually disappear, meanwhile a new absorption appears at 1417 cm^{-1} due to the tetrasubstituted benzene ring indicating that ring-opening of benzoxazine has occurred resulting in the formation of POSS-Pbz networks[20-22].

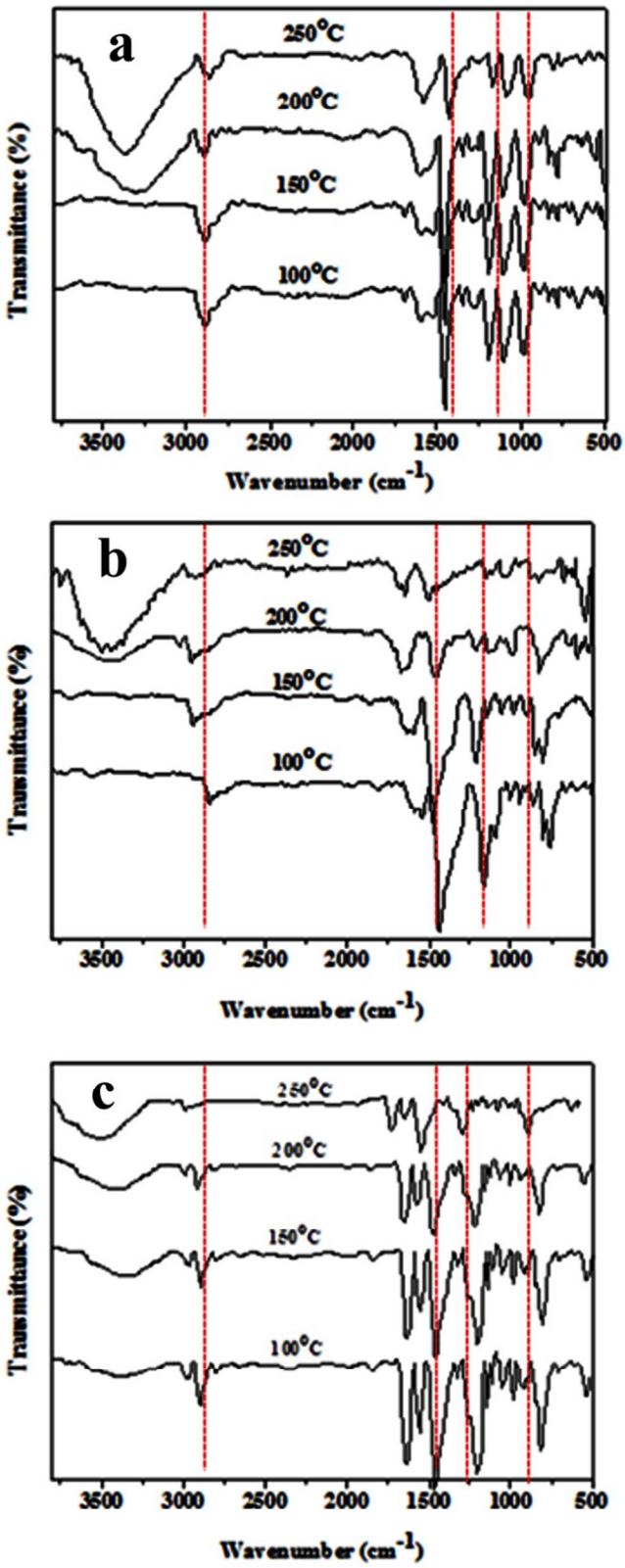

Figure 5 FTIR spectra showing curing behavior of POSS-Bzo monomers

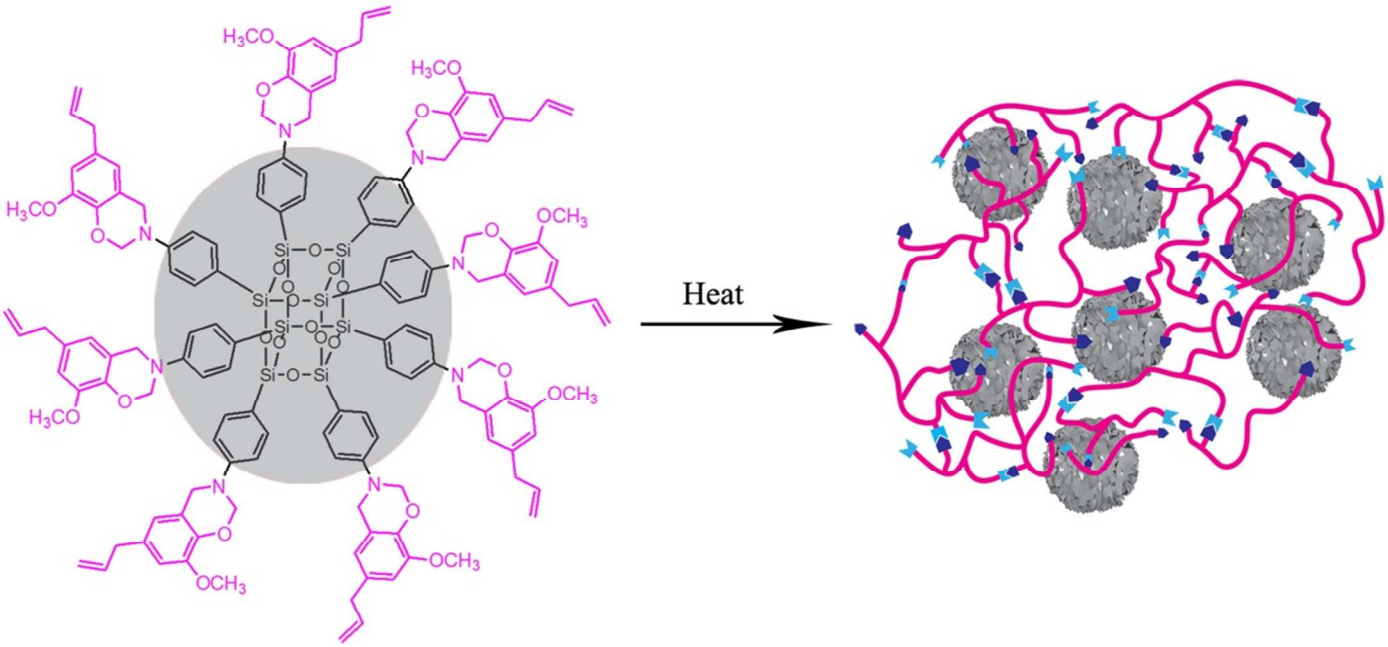

Scheme 4 Schematic representation showing the formation of POSS-EPbz nanocomposite

3.3. Morphological Studies

Scanning electron microscope (SEM) was used to investigate the morphology of the POSS-Pbz hybrid nanocomposites. Figure 6 displays SEM images of polybenzoxazine POSS nanocomposites [POSS-EPbz, POSS-GPbz and POSS-VPbz]. SEM micrographs of these hybrid nanocomposites indicate that the POSS moieties remained evenly dispersed within the polybenzoxazine matrix[23]. The degree of dispersion of the nanofiller plays an important role in influencing the properties of the resulting nanocomposites. Energy dispersive X-ray spectroscopy (EDX), integrated with scanning electron microscopy, was employed to analyze the elemental composition of the POSS-Pbz hybrids. The presence of carbon, nitrogen, oxygen and silicon offers a good measure of the presence of POSS and polybenzoxazine in the matrix as shown in Figure 7. Surface analysis of POSS-Pbz nanocomposites was carried out by AFM measurements[24]. Figure 8 displays the AFM images of POSS-EPbz, POSS-GPbz and POSS-VPbz respectively. These heterogeneous materials show the presence of two different domains, in which rough areas correspond to POSS rich domains, whereas smooth areas correspond to polybenzoxazine regions. When the stepwise polymerization begins, the benzoxazine monomer unit tends to react with other benzoxazine unit in its vicinity, thus preventing the formation of POSS aggregates in the matrix[25].

HR-TEM was performed to analyze the microstructure of POSS-Pbz nanocomposites (Figure 9). The figure shows dark spherical particles of about 5 to 10 nm in size which are uniformly dispersed in the POSS-Pbz networks. These dark portions are attributed to POSS nanoparticles. This is due to the high electron density of the POSS cages. Moreover, there is no aggregation of POSS moieties even after complete curing showing uniform distribution of POSS in these hybrid networks. Such uniform morphology is relevant in determining the ultimate properties of the nanocomposites[26].

3.4. Dielectric properties of POSS-Pbz nanocomposites

The dielectric constant and dielectric loss of the materials are directly related to the polarizability and porosity of the materials and are strongly dependent on their chemical structure. This phenomenon is due to the frequency dependence of polarization mechanisms[27]. As the frequency increases, there is a decrease in orientation polarization and dipole moment and so it takes longer time for electronic and ionic polarization to occur, thus resulting in a decrease of dielectric constant and loss value[28].

However, POSS-Pbz nanocomposites exhibit stable dielectric constant in wide frequency range. Figure 10 shows the frequency dependence of dielectric constant for the POSS-EPbz, POSS-GPbz and POSS-VPbz nanocomposites from 10 Hz - 1 MHz. The dielectric constant of all the samples decreases slightly with an increase in frequency. Figure 11 shows the dependence curves of the dielectric loss of the samples on frequency. The values of dielectric loss are fairly low with dielectric constants of 1.98, 1.85 & 1.88 for POSS-EPbz, POSS-GPbz and POSS-VPbz respectively at 1 MHz.

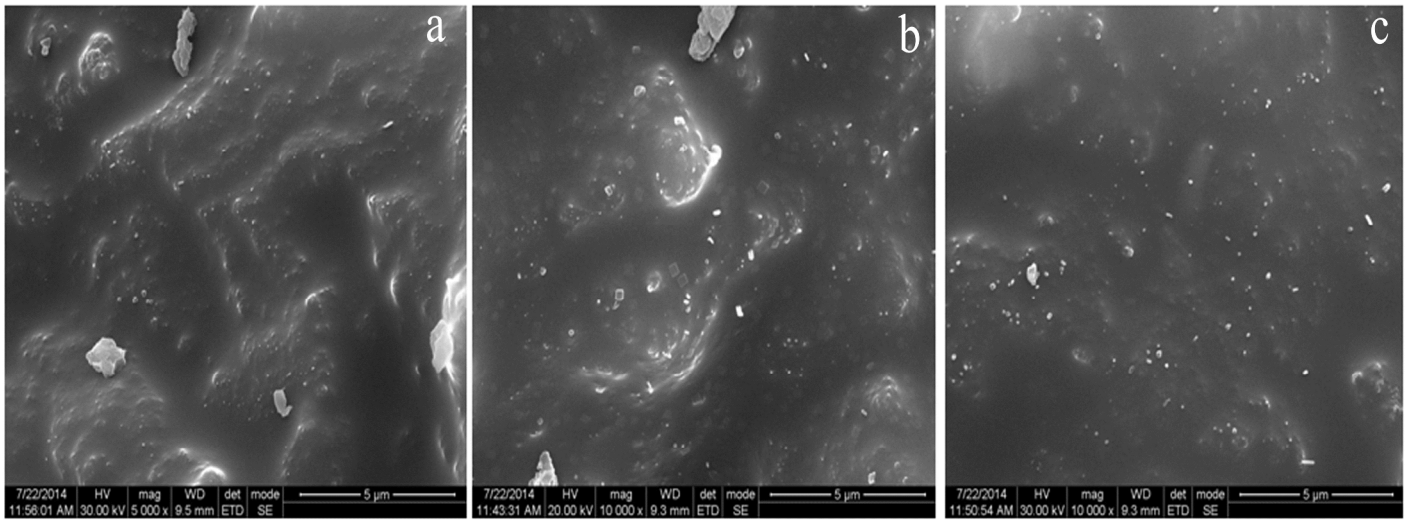

Figure 6 SEM images of the POSS-Pbz nanocomposites a) POSS-EPbz b) POSS-GPbz and c) POSS-VPbz

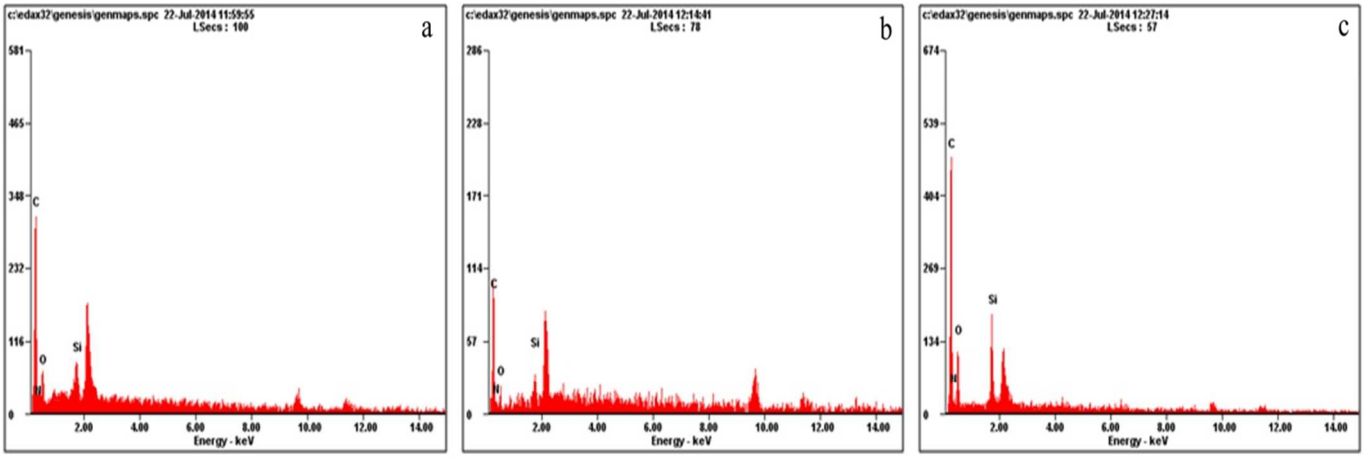

Figure 7 EDX of POSS-Pbz nanocomposites a) POSS-EPbz b) POSS-GPbz and c) POSS-VPbz

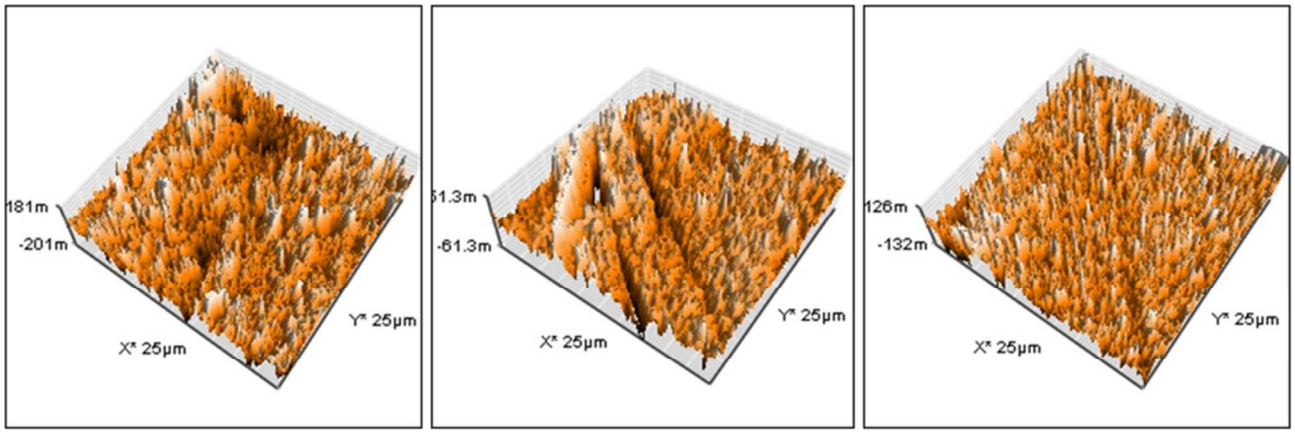

Figure 8 AFM images of the POSS-Pbz nanocomposites a) POSS-EPbz b) POSS-GPbz and c) POSS-VPbz

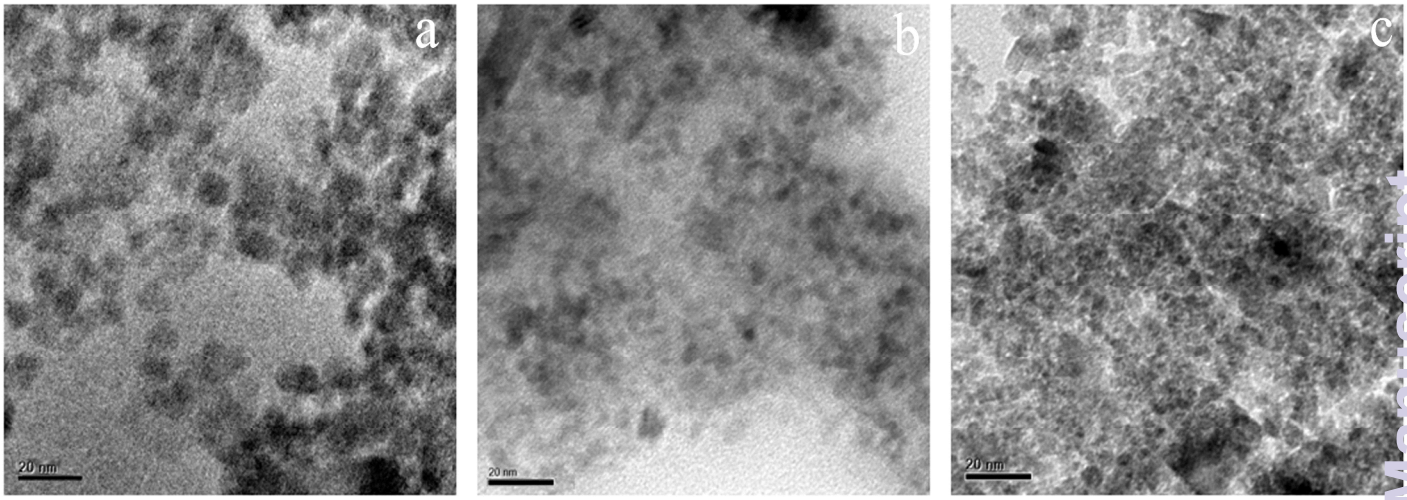

Figure 9 HRTEM images of the POSS-Pbz nanocomposites a) POSS-EPbz b) POSS-GPbz and c) POSS-VPbz

One possible reason for lower dielectric values is that the cubic silica core present in the POSS molecules are dispersed homogeneously in the matrix, thereby increasing the free volume. And the other is that the POSS molecule itself is a low polar molecule, which also might reduce the dielectric constant and loss values. These characteristic results indicate that the nanocomposites may have high potential application as microelectronic packaging materials[29].

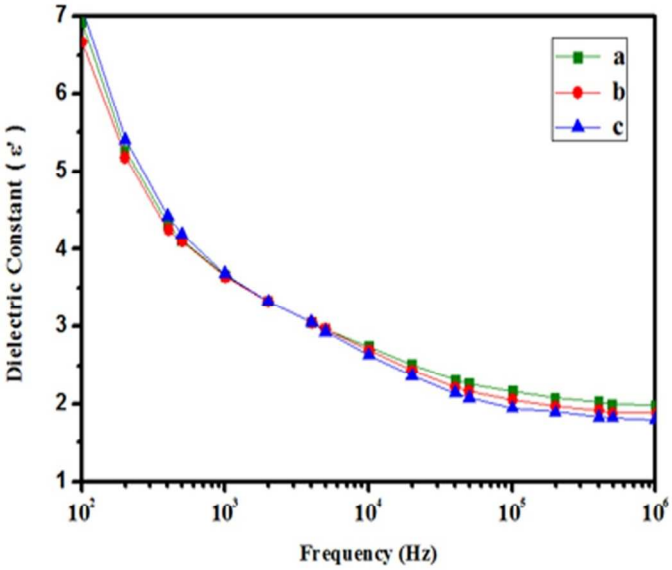

Figures 10 Dielectric constants of POSS-Pbz nanocomposites a) POSS-EPbz b) POSS-GPbz and c) POSS-VPbz

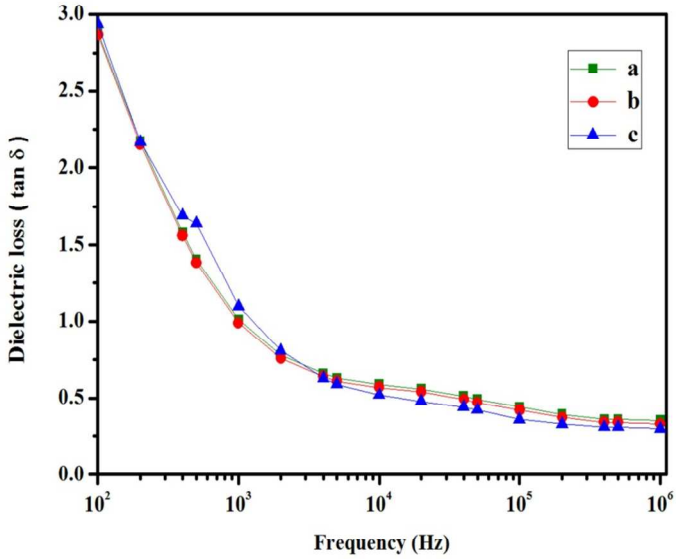

Figure 11 Dielectric loss of POSS-Pbz nanocomposites a) POSS-EPbz b) POSS-GPbz and c) POSS-VPbz

3.5. Dynamic mechanical analysis

The viscoelastic properties of POSS-Pbz nanocomposites were examined by DMA measurement. Figures 12 and 13 display the temperature dependence of G' and E' of POSS-EPbz, POSS-GPbz and POSS-VPbz nanocomposites and the data are summarized in Table 1. The G' for POSS-EPbz, POSS-GPbz and POSS-VPbz nanocomposites at 30 °C was found to be 2.63, 2.91 and 2.84 GPa respectively. It can be seen that there is an enhancement in dynamic properties of the nanocomposites when compared with eugenol based polybenzoxazine [G' of PBz-PHE: 5.3 MPa] [30]. This enhancement is due to the strong interaction

between its components, in which the POSS particles are covalently bonded to the benzoxazine units.

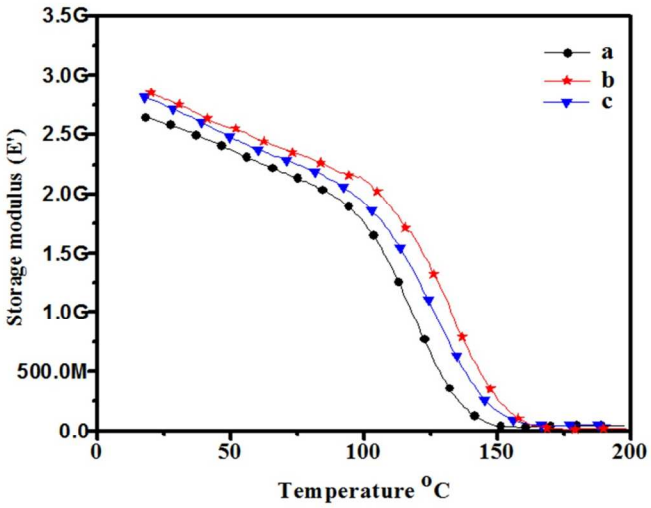

Figure 12 Storage moduli (from DMA measurements) of POSS-Pbz nanocomposites a) POSS-EPbz b) POSS-GPbz and c) POSS-VPbz

The bulky and rigid POSS nanoparticles, stiffen the cross-linked polybenxozazine network which significantly increases the E' value. On one hand, the nano reinforcement effect of POSS leads to suppression of molecular mobility in the polybenzoxazine matrix which tends to increase the modulus of the material[26,31]. On the other hand, the inclusion of POSS in the system will decrease the density of the nanocomposites. In these organic/inorganic hybrid materials, the cubic silsesquioxane core is rigid, and there are eight curable benzoxazine groups which are appended to the silsesquioxane core via Si-O linkages. In this kind of network structure, the value of T_g is related directly to the cross-linking density. The temperature at which the tan d curve has a maximum in the DMA plot represents the glass transition temperature of the material. Figure 13 reveals the T_g value of POSS-EPbz, POSS-GPbz and POSS-VPbz to be 118, 126 and 123 °C respectively. There is no appreciable difference in the glass transition temperature for the three prepared nanocomposites, due to the presence of crosslinked network structure. As a result, the glass transition temperatures of these nanocomposites remained approximately constant[32,33].

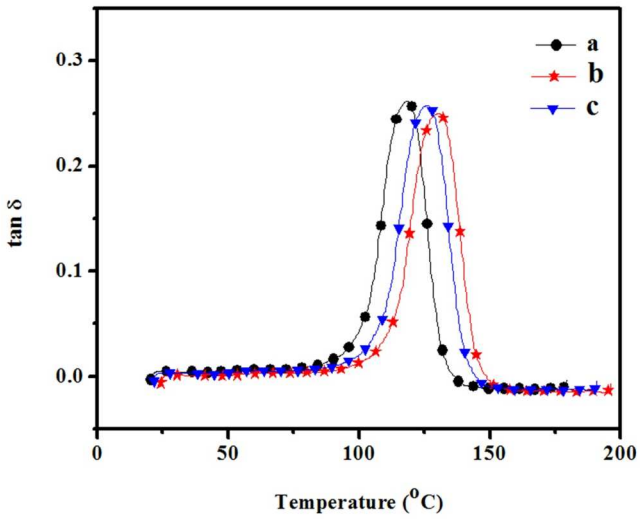

Figure 13 Loss moduli (from DMA measurements) of POSS-Pbz nanocomposites a) POSS-EPbz b) POSS-GPbz and c) POSS-VPbz

Table 1 Dielectric values, DMA data and cross-linking density of POSS-Pbz nanocomposites.

S.No.	Nano-composites	Dielectric constant (Ɛ') (1 MHz)	Dielectric loss (Ɛ") (1 MHz)	Ɛ' (GPa) At 30°C	T_g (°C)	$v_e \times 10^5$ (mol m^{-3}) At 30°C
1	POSS-EPbz	1.98	0.31	2.63	118	3.5
2	POSS-GPbz	1.85	0.28	2.91	126	3.8
3	POSS-VPbz	1.88	0.29	2.84	123	3.7

3.6. Crosslink density

The cross – link density or concentration of network chain, υ_e, is the number of moles of network chains per unit volume of the cured polymers. Crosslink density of highly crosslinked thermoset can be determined by modulus measurements in the rubbery plateau by using the equation of state for rubber elasticity[34] as,

$$\upsilon_e = E'/3RT$$

where,

E' = tensile storage modulus (DMA) in the rubbery plateau

T = temperature in K corresponding to the storage modulus value

R = gas constant

Table 1 shows the crosslink density of the POSS-Pbz nanocomposites. The enhancement in cross-link density is due to POSS macromonomers acting as nanosized cross-linker in the POSS-Pbz matrix[27,29,30].

3.7. Thermal stability of POSS-Pbz nanocomposties

Thermal stability and decomposition behavior of POSS-Pbzo nanocomposites were determined using TGA under nitrogen atmosphere. Figure 14 illustrates the weight loss curves of POSS-EPbz, POSS-GPbz and POSS-VPbz nanocomposites. Table 2 summarizes the data of T_i, $T_{5\%}$ and $T_{10\%}$ weight loss temperatures and char yield (CY) at 800 ^oC. The POSS-Pbzo nanocomposites show an initial and 10% degradation temperatures at 274 & 338 ^oC for POSS-EPbz; at 297 & 369 ^oC for POSS-VPbz; and at 303 & 371 ^oC for POSS-GPbz respectively. The degradation of POSS-EPbz occurs earlier when compared with the other two nanocomposites. This is due to the presence of allyl group in its structure. Whereas the presence of aldehyde group in POSS-VPbz nanocomposites degrades next, then followed by POSS-GPbz nanocomposites, which has fewer substituents in the aromatic ring when compared with the others[26,31,33].

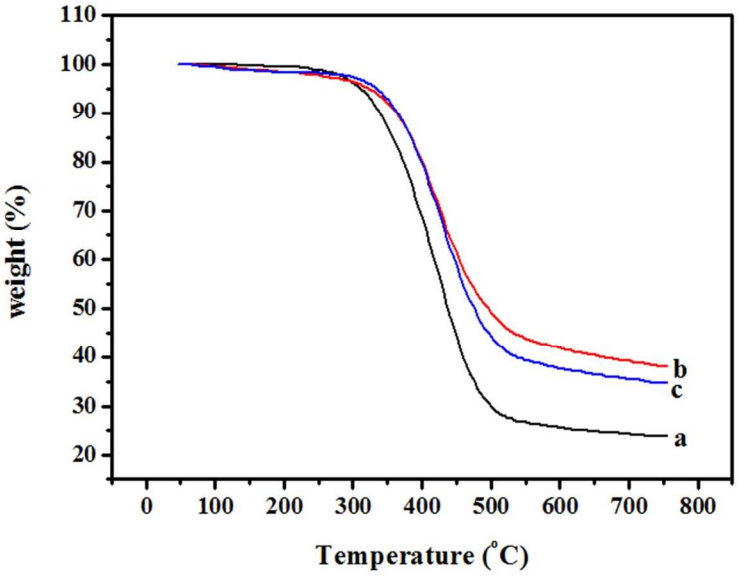

Figure 14 TGA curves of POSS-Pbz nanocomposites a) POSS-EPbz b) POSS-GPbz and c) POSS-VPbz

The limiting oxygen index (LOI) value, which is taken as an indicator to evaluate the polymer's flame retardancy[35] are given in Table 2. Char yield of a material can be used to estimate LOI according to Van Krevelen and Hoftyzer equation. LOI is defined as the minimum fraction of oxygen in a mixture of O_2 and N_2 that will support flaming combustion. The LOI values were calculated from the char yield resulted from TGA analysis by using Van Krevelan & Hofytzer equation[36,37] as shown below,

$$LOI = 17.5 + 0.4\ (CY)$$

where,

LOI = Limiting oxygen index

CY = Char yield (from TGA data)

Table 2 TGA data of POSS-Pbz nanocomposites

S.No.	Nano-composites	$T_{i\%}$	$T_{5\%}$	$T_{10\%}$	Charyield (%)	LOI values
1.	POSS-EPbz	274	311	338	24	27.1
2.	POSS-GPbz	303	339	371	38	32.7
3.	POSS-VPbz	297	327	369	36	31.9

3.8. Moisture absorption analysis

The absorbed moisture acts as a plasticizer, which not only reduces the mechanical and thermal properties of the polymers but also has a detrimental effect on dielectric property. Similarly water absorption also affects the dielectric property as it possesses large dielectric constant value of 78.5 at 25 ^oC. Hence, both the moisture and water absorptions should be below 1% for the material to be used in dielectric applications.

The moisture resistance of the prepared POSS-polybenzoxazine nanocomposites (POSS-EPbz, POSS-GPbz and POSS-VPbz) was studied in water & air and the obtained results are tabulated in Table 3. The percentage of weight change (from both water and air) for the specimen was determined using the following equation,

$$\text{Weight change (\%)} = \frac{W_2 - W_1}{W_1} \times 100$$

where, W_1 and W_2 are the weight (in gram) of the specimen before and after immersion in water respectively. The synthesized nanocomposites have low water and moisture absorptions (Table 3). POSS-Pbz nanocomposites generally possess low water absorption ability due to its high crosslink density and hydrophobic property[38].Their moisture absorptions are <0.01% in air atmosphere and between 0.05 to 0.03% under water environment. These low values are a result of high crosslink density of the polymer chains. These results indicate that the

POSS-Pbz nanocomposites possess an outstanding property to resist moisture uptake both in air and under water environment[39].

Table 3 Moisture absorption values of POSS-Pbz nanocomposites both in air and water environment

Environment	POSS-EPbz	POSS-GPbz	POSS-VPbz
In air 1 day	<0.01	<0.01	<0.01
In air 1 week	<0.01	<0.01	<0.01
In water 1 day	<0.01	<0.01	<0.01
In water 1 week	0.05	0.03	0.04

4. Conclusions

In conclusion, the article describes the successful synthesis, structural and thermal characterizations of benzoxazines based on renewable resources viz eugenol, guaiacol and vanillin with POSS entity. The reaction mechanism has been assessed by means of FT-IR and NMR measurements, evidencing the occurrence of benzoxazine ring attached to POSS molecules. The curing mechanism suggested that the formyl group of vanillin helps in curing of benzoxazine at a lower temperature (205 ^{o}C for POSS-VBz). Moreover, the storage modulus of the nanocomposites increased and Tg shifted to lower temperature of 231 ^{o}C for POSS-VPbz. The hybrid systems did not display phase heterogeneity as the octafunctional POSS moieties are dispersed well in the matrix. The HRTEM micrographs of the nanocomposites show POSS nanoparticles with 5 to 10 nm in size. The proposed POSS-Pbz nanocomposites from renewable sources have a great potential application as high-performance microelectronic package materials because of its excellent dielectric properties and thermal stability under high temperature.

Acknowledgement

The authors acknowledge the Department of Science and Technology, New Delhi and The Council of Scientific and Industrial Research for funding this project. The authors also acknowledge DST (FIST) and UGC (SAP) for the financial support extended to procure instrumental facilities.

Notes

Department of Chemistry, Anna University, Chennai–600 025, Tamilnadu, India. Fax: 044 2235 8651; Tel: 044 2235 8665; E-mail: tkpchem30@gmail.com

† Electronic Supplementary Information (ESI) available: [Supporting Scheme and Figures for FT-IR, ^{1}H & ^{13}C NMR and ^{29}Si NMR of OAPS are available in ESI]. See DOI: 10.1039/b000000x/

References

1. K. M. Lee, P. T. Knight, T. Chung and P. T. Mather, *Macromolecules*, 2008, **41**, 4730–4738.
2. B. Kiskan, N. N. Ghosh and Yusuf Yagci, *Polym. Int.,* 2011, **60**, 167–177.
3. K. D. Demir, M. A. Tasdelen, T. Uyar, A. W. Kawaguchi, A. Sudo, T. Endo and Y. Yagci, *J. Poly. Sci.,* 2011, **49**, 4213–4220.
4. E. Markovic, S. Clarke, J. Matisons and G. P. Simon, *Macromolecules,* 2008, **41**, 1685–1692.
5. K. Zhang, Q. Zhuang, X. Liu, G. Yang, R. Cai and Z. Han, *Macromolecules,* 2013, **46**, 2696–2704.
6. C. K. Chozhan, M. Alagar and P. Gnanasundaram, *Acta. Materialia.,* 2009, **57**, 782–794.
7. S. A. Garea, H. Iovu, A. Nicolescu and C. Deleanu, *Polymer Testing,* 2009, **28**, 338–347.
8. C.-M. Leu, Y.-T. Chang and K.-H. Wei, *Macromolecules,* 2003, **36**, 9122–9127.
9. A. Strachota, I. Kroutilova, J. Kovarova and L. Matejka, *Macromolecules,* 2004, **37**, 9457–9464.
10. N. K. Sini, J. Bijwe and I. K. Varma, *J. Polym. Sci.,* 2014, **52**, 7–11.
11. M. Verespej, Experts predict boom in bio-based resins, www.prw.com, 2013.
12. R. Tamaki, Y. Tanaka, M. Z. Asuncion, J. Choi and R. M. Laine, *J. Am. Chem. Soc.,* 2001, **123**, 12416–12417.
13. T. Agag, L. Jiu and H. Ishida, *Polymer,* 2009, **50**, 5940–5944.
14. Y. Liu, Z. Yue and J. Gao, *Polymer,* 2010, **51**, 3722–3729.
15. C. V. Mythili, A. M. Retna and S. Gopalakrishnan, *Bull. Mater. Sci.,* 2004, **27**, 235–241.
16. T. Agag and T. Takeichi, *Macromolecules,* 2003, **36**, 6010–6017.
17. S. Li, S. Yan, J. Yu and B. Yu, *J. Appl. Polym. Sci.,* 2011, **122**, 2843–2848.
18. A. Van, K. Chiou and H. Ishida, *Polymer,* 2014, **55**, 1443–1451.
19. J. Opfermann and E. Kaiserberger, *Thermochim. Acta.,* 1992, **203**, 167–175.
20. Z. Xiaoqing, M. G. Looney, D. H. Solomon and A. K. Whittaker, *Polymer,* 1997, **38**, 5835–5848.
21. Y.-C. Liu and C.-I. Chou, *J. Polym. Sci. Part A: Polym. Chem.,* 2005, **43**, 5267–5282.
22. J.-M. Huang, S.-W. Kuo, H.-J. Huang, Y.-X. Wang and Y.-T. Chen, *J. Appl. Polym. Sci.,* 2009, **111**, 628–634.
23. C. Zuniga, M. S. Larrechi, G. Lligadas, J. C. Ronda, M. Galià and V. Cádiz, *Polym. Degrad. Stab.,* 2013, **98**, 2617–2626.
24. Y.-J. Lee, S.-W. Kuo, Y.-C. Su, J.-K. Chen, C.-W. Tu and F.-C. Chang, *Polymer,* 2004, **45**, 6321–6331.
25. J. Zhang, R. Xu and D. Yu, *Eur. Polym. J.,* 2007, **43**, 743–752.
26. G. Yang, Z. Xue, Q. Zhunag, X. Liu, K. Zhang and Z. Han, *Synthetic Metals,* 2013, **175**, 112–119.
27. Y.-J. Lee, J.-M. Huang, S.-W. Kuo, J.-K. Chen and F.-C. Chang, *Polymer,* 2005, **46**, 2320–2330.
28. C. Liu, D. Shen, R. M. Sebastian, J. Marquet and R. Schonfeld, *Macromolecules,* 2011, **44**, 4616–4622.
29. L. Marta, P.-S. Mercedes, A.-G. Francisco and S. Roberto, *J. Mater. Chem.,* 2011, **21**, 12803–12811.
30. P. Thirukumaran, A. Shakila Parveen and M. Sarojadevi, *RSC Adv.,* 2014, **4**, 7959–7966.
31. K.-W. Huang and S.-W. Kuo, *Macromol. Chem. Phys.,* 2010, **211**, 2301–2311.
32. Q. Chen, R. Xu, J. Zhang and D. Yu, *Macromol. Rapid Commun.,* 2005, **26**, 1878–1882.

33. D. Wenjie, S. Jiajia, W. Yixian, X. Riwei and Y. Dingsheng, *Materials and Design,* 2010, **31**, 1720–1725.
34. V.-H. Pedro, D. Kazuo, A. Hiroshi and H. Ishida, *Macromolecules,* 2008, **41**, 9704–9714.
35. C.-L. Chiang and C.-C. M. Ma, *Polym. Degrad. Stab.,* 2004, **83**, 207–214.
36. M. Sponton, G. Lligadas, J. C. Ronda, M. Galia and V. Cadiz, *Polym. Degrad. Stab.,* 2009, **94**, 1693–1699.
37. D.W. Van Krevelen, *Polym. J.,* 1975, **16**, 615–620.
38. Nalwa, Hand book of advance electronic and photonic materials and devices, Vol.4, San Diego, Academic Press (2001).
39. H. Ishida and H. Y. Low, *Macromolecules,* 1997, **30**, 1099–1106.